Catalysis Today 296 (2017) 127–134

Contents lists available at ScienceDirect

Catalysis Today

journal homepage: www.elsevier.com/locate/cattod

Kinetic and mechanistic study of the synthesis of ionone isomers from pseudoionone on Brønsted acid solids

V.K. Díez*, C.R. Apesteguía, J.I. Di Cosimo

Catalysis Science and Engineering Research Group (GICIC), INCAPE, UNL-CONICET, CCT CONICET Santa Fe, Colectora Ruta Nac. 168, km 0, Paraje "El Pozo", (3000) Santa Fe, Argentina

ARTICLE INFO

Keywords:
Ionones
Pseudoionone
Brønsted acid solids
HPA/SiO_2 catalysts
TFA/SiO_2 catalysts
Kinetic modeling

ABSTRACT

The kinetics of the liquid-phase synthesis of α-, β- and γ-ionones from pseudoionone was studied on Brønsted acid solids. Four silica-supported tungstophosphoric acid catalysts containing different heteropolyacid loadings, as well as a silica-supported triflic acid sample and a commercial resin (Amberlyst 35W) were tested in a batch reactor at 343–383 K under autogenous pressure.

The final composition of the ionone isomer mixture depended on the catalyst acidic properties and operational conditions. The reaction pathways leading to the three ionone isomers were elucidated by postulating a heterogeneous Langmuir-Hinshelwood-Hougen-Watson (LHHW) kinetic model. First order rate expressions, participation of a single Brønsted acid site in each reaction step and a cationic cyclic intermediate shared by the three ionone isomers were the main model assumptions. It was found that α-, β- and γ-ionones form directly from pseudoionone by cyclization. However, the final concentration of α- and β-ionones is enhanced in consecutive pathways involving the isomerization of γ-ionone. The relative importance of the isomerization steps and the selective formation of α- or β-ionone depend on the Brønsted acid site strength and reaction temperature.

1. Introduction

Ionones (α, β and γ isomers) are widely used as pharmaceuticals and fragrances. The β-ionone isomer is used in the synthesis of vitamin A, while α- and γ-ionones are appreciated in the fragrance and cosmetic industries for their violet and fruity-woody scent, respectively [1,2]. The current commercial synthesis of ionones from citral takes place via a homogeneously catalyzed two-step process. Firstly, pseudoionone (PS) is obtained by aldol condensation of citral with acetone in the presence of diluted bases. Then, ionones are produced by cyclization of PS using strong mineral acids (H_2SO_4, H_3PO_4) as catalysts [3]. However, the use of mineral bases and acids entails concerns related to high toxicity, corrosion, and disposal of spent catalysts. Thus, in recent years new strategies have been postulated in the literature for ionone production in which liquid bases and acids are replaced by solid catalysts.

Time ago, we explored the second reaction step, i.e., the cyclization of PS to ionones on several solid acids such as unsupported tungstophosphoric acid (HPA), silica-supported HPA (HPAS), silica-supported triflic acid (TFAS), Cs-HPA, zeolite HBEA, SiO_2-Al_2O_3 and a commercial Amberlyst 35W resin [4–6]. The acidic nature (Lewis or Brønsted) of the active sites required for selective ionone synthesis was initially investigated [4]. In addition, the effect of the HPA loading and reaction conditions (temperature and reaction time) on catalytic activity and selectivity was studied on HPAS catalysts [5]. Finally, we investigated the effect of the acid site strength on ionone isomer selectivity by comparing the catalytic performance of three different Brønsted acid catalysts (HPAS, TFAS and Amberlyst 35W) [6]. The main findings of these previous works were that the reaction is efficiently promoted on catalysts containing a high density of strong Brønsted acid sites such as those of HPAS, TFAS, and Amberlyst 35W. In contrast, PS conversion was poorly promoted on Lewis acids such as SiO_2-Al_2O_3. In addition, it was found that ionone synthesis is favored at high reaction temperatures on HPAS catalysts so that the ionone yields at 383 K are comparable to those obtained by homogeneous catalysis using concentrated sulfuric acid.

Although the kinetic and mechanistic features of the ionone synthesis from PS have been investigated using homogeneous acid catalysis [7,8], they have not been discussed in detail using solid catalysts. In this work we investigate the kinetics and reaction mechanism involved in the formation of the three ionone isomers from PS on Brønsted acid solid catalysts. The kinetic performance of HPAS,

* Corresponding author.
E-mail address: verodiez@fiq.unl.edu.ar (V.K. Díez).

http://dx.doi.org/10.1016/j.cattod.2017.04.068
Received 3 January 2017; Received in revised form 22 March 2017; Accepted 30 April 2017
Available online 26 May 2017

TFAS and Amberlyst 35W catalysts was compared. In particular, we tested HPAS catalysts with different HPA loadings and at different temperatures. The reaction pathways leading to the different ionone isomers were discussed as well as how the selective formation of a particular isomer is affected by the catalyst acidic properties and reaction conditions. A complex reaction network was postulated and a heterogeneous Langmuir-Hinshelwood-Hougen-Watson (LHHW) kinetic model was proposed to interpret the catalytic data. Several kinetic parameters were calculated and statistically validated. The dependence of the kinetic parameters on the reaction temperature and catalyst acid properties was elucidated. The kinetic model successfully interprets the liquid-phase synthesis of ionone isomers promoted by different Brønsted acid solids.

2. Experimental

2.1. Catalyst synthesis

Four HPA/SiO_2 catalysts with different HPA loadings (18.8, 26.6, 42.5 and 58.5 wt.%) were previously prepared by the incipient wetness impregnation method [5]. The tungstophosphoric acid ($H_3PW_{12}O_{40}.xH_2O$, Merck, GR) was added to a commercial SiO_2 (Grace Davison, G62, 99.7) using aqueous solutions of HPA. Also, a silica-supported triflic acid catalyst (TFA/SiO_2) with an acid content of 8.0 wt.% was prepared by the same procedure using an aqueous solution of commercial TFA (CF_3SO_3H, Sigma-Aldrich, Reagent Grade). Details are given elsewhere [6]. The impregnated samples were dried at 353 K and then decomposed and stabilized at 523 K (HPA/SiO_2) and 383 K (TFA/SiO_2) for 18 h in N_2 (40 cm^3/min). The resulting silica-supported acid catalysts were denoted as HPAS-x and TFAS, where x is the HPA content expressed in wt.%. Amberlyst 35W resin pellets (Rohm and Haas) were crushed and sieved to retain particles between 180 and 480 μm. The resin was treated in N_2 (40 cm^3/min) at 373 K overnight before use.

2.2. Catalyst characterization

Chemical and spectroscopic techniques employed during catalyst characterization were thoroughly described in previous works [5,6]. BET surface areas (*SA*) were measured by N_2 physisorption at 77 K using an Autosorb Quantachrome 1-C sorptometer. Structural properties of HPAS-x samples were determined by X-ray diffraction (XRD) between 20° and 80° using a Shimadzu XD-D1 diffractometer equipped with Cu Kα radiation and a Ni filter. The chemical content of HPA in the calcined HPAS-x catalysts was determined by monitoring the tungsten content in a UV–vis spectrometer (Metrolab 1700). This quantitative method involves the calcination of the sample in an oven at 1073 K in order to transform $H_3PW_{12}O_{40}xH_2O$ in tungsten oxide (WO_3) and the subsequent digestion in an alkali solution. The solution containing WO_3 was finally analyzed by the UV–vis technique. More details are given elsewhere [9]. The TFA loading in the TFAS sample was measured by titration of the sample protons [6]. TFAS (0.3 g) was suspended in 75 ml of an aqueous solution of KCl (0.03 M) to release the triflic acid protons to the aqueous solution. The suspension was stirred for 20 min and then titrated with a 0.06 M KOH solution using phenolphthalein as the acid-base indicator.

The total acid site number (n_a, μmol/g) of HPAS-x samples was quantified by TPD of NH_3 preadsorbed at 373 K. Samples were thermally treated in He at 523 K, cooled down to 373 K and then exposed to a 1.01% NH_3/He flow to enable surface saturation. Weakly adsorbed NH_3 was removed by flushing with He. Finally, the sample temperature was increased from 373 K to 1073 K in a He flow. NH_3 concentration in the reactor effluent was monitored by a mass spectrometer (MS) detector in a Baltzers Omnistar unit. More experimental details are given elsewhere [5].

The chemical nature of surface acid sites was determined by Infrared Spectroscopy (IR) of pyridine adsorbed at room temperature and evacuated at increasing temperatures using a Shimadzu FTIR Prestige-21 spectrophotometer. Details are given elsewhere [6].

2.3. Catalytic testing

The liquid-phase cyclization of pseudoionone, PS (Fluka, > 95%) was carried out at 343–383 K under autogenous pressure (250 kPa) in a batch Parr reactor, using dehydrated toluene as a solvent with typically a Toluene/PS = 71 molar ratio and a catalyst/PS = 28–56 wt.% ratio.

Before the catalytic test, catalysts were thermally treated ex-situ in a N_2 stream at the calcination temperature for 2 h to remove adsorbed water. After introducing the reactant mixture the reactor was sealed and flushed with N_2 and then the mixture was heated up to the reaction temperature under stirring (300 rpm). The catalyst powder was added to the reaction mixture to start the reaction. Reaction products were periodically analyzed during the 6-h reaction in a Varian Star 3400 CX gas chromatograph equipped with a FID and a Carbowax Amine 30 M capillary column. Main reaction products were ionones (α, β and γ isomers); in some experiments, unidentified compounds were detected in a concentration lower than 10%.

2.4. Kinetic modeling and statistical analysis

The reaction mechanism of the liquid-phase synthesis of α-, β- and γ-ionones from pseudoionone (PS) on Brønsted acid solids was studied using a heterogeneous Langmuir-Hinshelwood-Hougen-Watson (LHHW) kinetic model. The differential equations were solved numerically using the Runge-Kutta-Merson algorithm. The relative molar concentrations of all the species over the course of reaction were calculated and compared with the experimental values. The model parameter estimation was performed by non-linear regression, using a Levenberg-Marquardt algorithm, which minimizes the sum of the squared errors (*SSE*) [10] between the experimental data and the data predicted by the model according to Eq. (1):

$$SSE = \sum_{i=1}^{n} (C^*_{jcalc} - C^*_{jobs})^2 \quad (1)$$

where C^*_j is the relative concentration of compound j (C_j/C^0_{PS}), C^0_{PS} is the concentration of pseudoionone in the reactor at $t = 0$ and C^*_{jcalc} is the value calculated by applying the model, which is compared with the experimental value (C^*_{jobs}).

The coefficient of determination (R^2) gives the fitting quality [10] and was calculated using Eq. (2):

$$R^2 = \frac{\sum_{i=1}^{n} (C^*_{jcalc} - \overline{C}^*_{jobs})^2}{\sum_{i=1}^{n} (C^*_{jobs} - \overline{C}^*_{jobs})^2} \quad (2)$$

where $\overline{C}^*_{jobs}$ is the mean of measured values.

The discrimination between models was carried out using the model selection criterion (*MSC*) [11], according to Eq. (3):

$$MSC = \ln\left[\frac{\Sigma (C^*_{jobs} - \overline{C}^*_{jobs})^2}{\Sigma (C^*_{jobs} - C^*_{jcalc})^2}\right] - \frac{2p}{m} \quad (3)$$

where p is the number of parameters; m is the number of experimental observations. The *MSC* parameter is used to compare different models and results independent of the magnitude (scaling) of the data. When comparing different models, the larger the *MSC* value, the better the fit and the more appropriate the model for interpreting the data.

Table 1
Surface area and acid properties of HPAS-x samples, TFAS and Amberlyst 35W [5,6].

Catalyst	*SA* (m^2/g)	Acid site number	
		n_a[a] (μmol/g)	n_{H+} (μmol/g)
SiO_2	272	0	–
HPAS-19	208	229	200[b]
HPAS-27	203	258	280[b]
HPAS-43	155	377	440[b]
HPAS-59	144	566	610[b]
HPA	9	534	1040[c]
TFAS	245	–	540 [d]
Amberlyst 35W	39	–	5200[e]

[a] By TPD of NH_3.
[b] By UV spectroscopy analysis.
[c] Calculated as H^+ per HPA unit.
[d] By acid-base titration.
[e] From manufacturer information.

3. Results and discussion

3.1. Catalyst characterization

The HPAS-x and TFAS catalysts were prepared by incipient wetness impregnation of commercial SiO_2 followed by thermal treatment in a N_2 flow. They were analyzed by several techniques in order to study their chemical, structural, textural and acid properties. A detailed discussion of characterization results can be found in previous works [5,6]. The most relevant results are summarized in Table 1.

The presence of the HPA structure in HPAS-x samples after impregnation and calcination was confirmed by comparing the XRD pattern of the samples with that of pure HPA (not shown here, see previous work [5]). On the other hand, the presence of triflic acid on the TFAS sample was investigated by monitoring the IR SO_2^{2-} vibration band at 1417 cm^{-1}, which is regarded as the characteristic band of supported triflic acid [12].

As was previously reported, the HPAS-x catalysts show surface areas in the range of 144–208 m^2/g [5]. The HPAS-x surface area values are lower than that of the commercial silica (272 m^2/g) and decrease with increasing HPA loading. Partial blocking of the silica pores by HPA moieties is probably responsible for this effect. In contrast, impregnation of SiO_2 with less bulky triflic acid causes only a slight decrease of the silica surface area from 272 to 245 m^2/g.

The surface acid properties of HPAS-x catalysts by combining TPD of NH_3 preadsorbed at 373 K and FTIR of pyridine adsorbed at room temperature were also investigated in a previous work [5]. Characterization of TFAS sample by TPD of NH_3 was not possible due to the low thermal stability of triflic acid on the silica surface caused by the low boiling point of this species (435 K). Similar reasons hindered characterization of Amberlyst 35W by TPD of NH_3 or FTIR of adsorbed pyridine.

On HPAS-x samples, the total amount of desorbed NH_3 was taken as an indication of the total number of surface acid sites, n_a. The resulting n_a values and the proton contents (n_{H+}, μmol H^+/g cat, measured by UV spectroscopy) are reported in Table 1. A good agreement was found between n_{H+} and n_a values, indicating that the HPA protons are completely accessible for NH_3 adsorption, even on samples containing high HPA loadings. Results of Table 1 also show an increase of both n_{H+} and the n_a as the heteropolyacid loading on HPAS-x samples increases. On the other hand, the n_a value measured for unsupported HPA was similar to that of HPAS-59 sample, what suggests that only a part of the acid sites of the three-dimensional structure of unsupported HPA is available for NH_3 adsorption.

Previously, the chemical nature of surface acid sites of HPAS-x and TFAS was determined from the IR spectra of pyridine preadsorbed at room temperature and evacuated at 423 K for HPAS-x samples and 353 K for TFAS [5,6]. The obtained spectra (not shown here, see previous works [5,6]) exhibit the IR band typical of pyridinium ion formed on Brønsted acid sites at 1537 cm^{-1} and also bands at 1636, 1608, and 1485 cm^{-1} [13]. Thus, these results confirm the findings by UV spectroscopy and acid-base titration on HPAS-x and TFAS samples respectively, regarding that these are essentially Brønsted acid solids. In particular, on the HPAS-x samples, the area under the band at 1537 cm^{-1} increases with the HPA content.

3.2. Ionone synthesis on Brønsted acid solids

3.2.1. Catalytic results on HPAS-x, TFAS and Amberlyst resin

A detailed discussion of catalytic results obtained on HPAS-x, TFAS and Amberlyst resin can be found in previous works [5,6]. Thus, a summary of the most relevant results will be presented below.

The time evolution of the relative concentration of pseudoionone and ionones obtained on HPAS-59, TFAS and Amberlyst 35W at 353 K are presented in Fig. 1. All catalysts showed high PS conversion (X_{PS}) values after the 6-h run (X_{PS} = 93-100%). Three ionone isomers (α, β and γ, Scheme 1) were detected. The nonzero initial slopes of the C_j/C^0_{PS} curves for the ionone isomers indicate that the three ionones are primary products formed directly from pseudoionone (PS) on the three catalysts. Fig. 1 also shows that the relative concentration of α-ionone monotonically increases with reaction time on the three catalysts. The same occurs with the β-ionone concentration curve on the TFAS sample. In contrast, the γ-ionone curve reaches a maximum on TFAS and Amberlyst 35W, suggesting that on these catalysts γ-ionone is consecutively converted to the other isomers.

From the results of Fig. 1, the initial ionone formation rate (r^0_{IONONE}, mmol/hg) was measured from the total ionone concentration

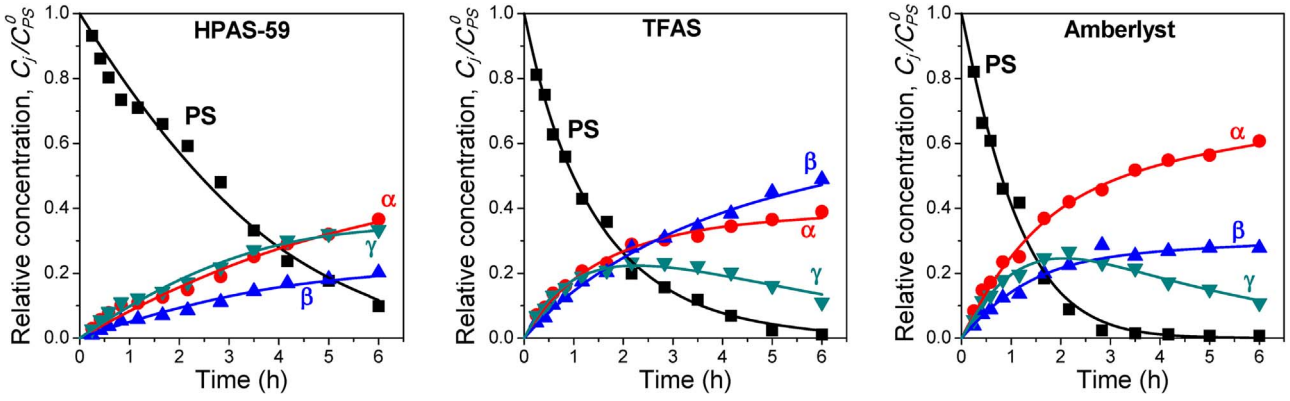

Fig. 1. Relative concentrations (C_j/C^0_{PS})as a function of reaction time on HPAS-59, TFAS and Amberlyst 35W catalysts. Symbols: experimental data; Lines: modeling results [353 K; Toluene/PS = 71 (molar ratio); $W_{HPAS-59} = W_{Amberlyst} = 1.0$ g; $W_{TFAS} = 0.5$ g].

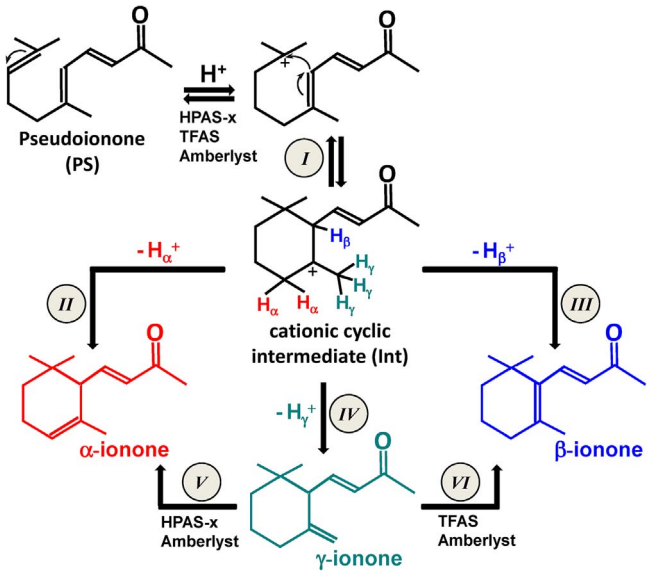

Scheme 1. Reaction steps for cyclization of pseudoionone to α-, β- and γ-ionones on Brønsted acid solids.

Table 2
Catalytic results obtained on Brønsted acid solids [5,6].

Entry	Catalyst	r^0_{IONONE} (mmol/h g)	Ionone isomer distribution at $X_{PS} \cong 70\%$ (%)		
			α	β	γ
1	SiO_2	0.0	–	–	–
2	HPAS-19	1.11	–	–	–
3	HPAS-27	2.82	34.1	19.9	46.0
4	HPAS-43	3.27	37.0	20.5	42.5
5	HPAS-59	4.48	37.7	21.6	40.7
6	HPA	0.06	–	–	–
7	TFAS	11.56	36.2	30.5	33.3
8	Amberlyst 35W	6.61	43.0	23.4	33.6

Reaction conditions: T = 353 K, P = 250 kPa, n^0_{PS} = 0.009 mol, Toluene/PS = 71 (molar ratio), $W_{HPAS-x} = W_{Amberlyst} = 1.0$ g, $W_{TFAS} = 0.5$ g.

($C_{IONONE} = C_\alpha + C_\beta + C\gamma$, not shown) versus time curve using Eq. (4), where W is the catalyst load:

$$r^0_{IONONE} = \frac{C^0_{PS}}{W}\left[\frac{d\,(C_{IONONE}/C^0_{PS})}{dt}\right]_{t=0} \quad (4)$$

The resulting r^0_{IONONE} values are given in Table 2, entries 5, 7 and 8. The activity order for ionone synthesis (TFAS > Amberlyst resin > HPAS-59) clearly does not correlate with n_{H+} (Table 1). Thus, in a previous work we concluded that, for solids with different chemical nature, the activity is probably the result of a combined effect of available acid sites and proton site strength [6]. The turnover frequency ($TOF = r^0_{IONONE}/n_{H+}$) values for the three samples seem to confirm it since for the TFAS sample a value of 21.4 h^{-1} was calculated in contrast to 7.3 h^{-1} and 1.3 h^{-1} for HPAS-59 and the resin, respectively. This *TOF* trend follows the acid strength order predicted by the Hammett acidity function ($-H_0$) indicating that the acidity of the triflic acid protons is stronger ($-H_0$ = 14.6), compared to those of tungstophosphoric acid (HPA) ($-H_0$ = 13.2) and Amberlyst 35W ($-H_0$ = 5.6) [14–16].

The initial ionone isomer distribution was similar on all samples giving a α:β:γ isomer ratio of approximately 40:20:40. As shown in Fig. 1, the ionone isomer distribution changes with reaction time and is strongly dependent on the catalyst Brønsted acid site strength; this is illustrated in Table 2, where the isomer distribution is compared at $X_{PS} \cong 70\%$. On HPAS-59, the contribution of each ionone isomer at $X_{PS} \cong 70\%$ is similar than the initial α:β:γ isomer ratio while on Amberlyst 35W the isomer mixture is enriched in α-ionone; on TFAS, the most strongly acid catalyst, β-ionone reaches the highest contribution (≅30%).

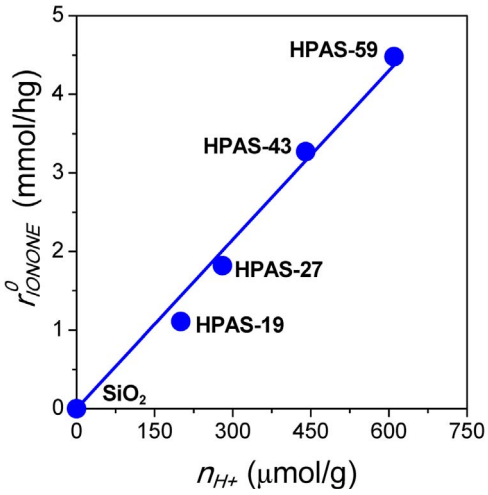

Fig. 2. Initial ionone formation rate (r^0_{IONONE}) as a function of the proton content on HPAS-x catalysts [353 K; Toluene/PS = 71 (molar ratio); 1.0 g of catalyst].

3.2.2. Effect of HPA content in HPAS-x catalysts

Four HPAS-x samples with HPA loadings of 18.8, 26.6, 42.5 and 58.5 wt.% were previously prepared, characterized and tested at identical reaction conditions in order to investigate the effect of the heteropolyacid content on the HPAS-x activity [5]. Pure SiO_2 and bulk HPA were also tested for comparative purposes. Results are presented in Table 2. The SiO_2 support was inactive for PS conversion to ionones because of the lack of acidic properties (Table 1). Bulk unsupported HPA showed low initial ionone formation rate (Table 2, entry 6) in spite of the fact that contains the highest number of Brønsted acid sites (Table 1). This result can be explained by considering that the compact three-dimensional structure of bulk HPA hinders the access of the PS molecules to the active centers of the solid.

The effect of the HPA content on the catalyst activity is shown in Fig. 2. Clearly, the linear correlation between initial ionone formation rate (r^0_{IONONE}) and the number of Brønsted acid sites (n_{H+}) suggests that the latter are involved in the kinetically relevant reaction steps of the ionone synthesis.

The effect of the HPA content on the product distribution at $X_{PS} \cong 70\%$ was also investigated, Table 2. It seems that the effect of increasing the HPA loading in the HPAS-x samples is limited to the activity enhancement of Fig. 2; the isomer distribution at 353 K is similar on the different HPAS-x samples (Table 2) and close to the initial α:β:γ isomer ratio (40:20:40). Thus, the results of Table 2 suggest that for HPA-based samples the selectivity to the different ionone isomers is independent of the number of surface acid sites.

3.2.3. Effect of the reaction temperature in HPAS-x catalysts

The effect of reaction temperature on activity and ionone isomer distribution was studied in the range of 343–383 K using the HPAS-x catalysts in a previous work [5]. Sample HPAS-59 was chosen for this study since according to Fig. 2, this is the most promising catalyst of the HPA-based series.

The time evolution of the relative concentrations of PS and ionone isomers can be compared at different temperatures in Fig. 3. Results show that the PS conversion increases with temperature and that above 363 K PS is completely converted before the end of the catalytic run.

On the other hand, the α-ionone concentration curve monotonically increases with time regardless of the reaction temperature whereas the β isomer curve levels off at high reaction times. Contrarily, the

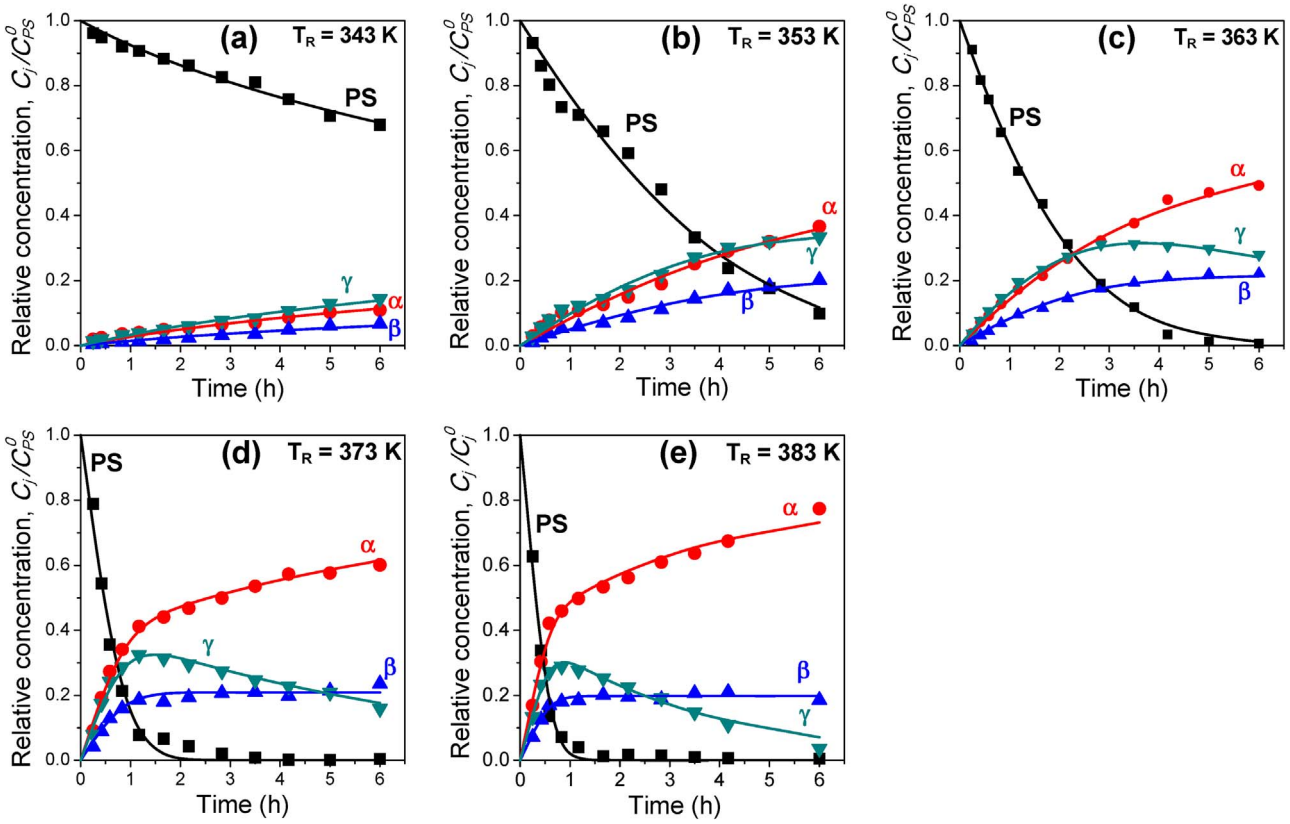

Fig. 3. Relative concentrations (C_j/C^0_{PS}) as a function of time on HPAS-59 at different reaction temperatures. (a) 343 K; (b) 353 K; (c) 363 K; (d) 373 K; (e) 383 K. Symbols: experimental data; Lines: modeling results [Toluene/PS = 71 (molar); 1.0 g of catalyst].

maximum of the γ isomer curve remarkably shifts to lower times with increasing temperatures, thereby suggesting that γ-ionone is an intermediate that converts to other isomers.

The effect of the reaction temperature on the selectivity was investigated by plotting the ionone isomer distribution at different temperatures and at $X_{PS} \cong 40\%$ [5]. Those results showed that at PS isoconversion the contribution of α-ionone increases from 35 to 45.2% at the expense of γ-ionone as the reaction temperature increases from 343 to 383 K. Thus, at high reaction temperatures α-ionone is the main product on HPAS-59. A similar result was obtained by Rachwalik et al. [17] using HPA/SiO_2 and HPA/SBA-15 catalysts. The analysis of the dependence of β isomer concentration with reaction temperature showed that β-ionone contribution remains almost constant at increasing temperatures taking values around 20%; that result confirmed that β-ionone is a primary and terminal product on HPA-based samples and that isomer interconversion is limited to isomerization of the γ isomer toward α-ionone.

3.2.4. *Reaction pathway for the synthesis of ionones on Brønsted acid solids*

Based on the results of Figs. 1 and 3 and previous works [5,6], a reaction pathway for the conversion of PS to ionones on Brønsted acid solid catalysts is postulated in Scheme 1. Firstly, the PS molecule is protonated as a result of the interaction with surface Brønsted acid sites leading to a common cationic cyclic intermediate (Int, Scheme 1, step *I*). From this cyclic intermediate the three ionone isomers are then formed in parallel pathways via proton detachment (steps *II*, *III* and *IV* in Scheme 1). Intermediate Int is rapidly converted on the surface to adsorbed ionone isomers after forming from PS; as a result, ionones are detected as primary products in the liquid phase in Figs. 1 and 3.

In the structure of the cyclic intermediate, three different kinds of hydrogen atoms coexist: H_α (two), H_β (one) and H_γ (three). These different protons must be detached to form α-, β- and γ-ionone, respectively. Taking into account the chemical structure of the ionone molecules, the following stability order can be speculated for the three ionone isomers: β > α > γ-ionone. The high stability of the β isomer is due to the extended system of conjugated C=C double bonds.

As discussed above, an isomer interconversion can be expected on the different catalysts as shown in Figs. 1 and 3, in particular at high reaction temperatures. Thus, on Amberlyst 35W and HPA-x catalysts the α isomer is probably formed not only from PS but also by isomerization of the C=C double bond of the least stable isomer (γ-ionone) in a consecutive step (Scheme 1, step *V*). Formation of the β isomer in significant amounts is more demanding than that of the other isomers since requires strong surface acid sites (as those present on TFAS). Also, the high stability of this isomer explains why β-ionone is not transformed into the other ionones by isomerization. Therefore, the shape of the curves of Fig. 3 suggests that on HPAS-x β-ionone forms exclusively from PS, as discussed in Section 3.2.3. Contrarily, on TFAS and Amberlyst 35W a contribution of the secondary pathway (γ-ionone isomerization, Scheme 1, step *VI*) can be expected taking into account the shape of the γ-ionone curves in Fig. 1.

3.3. *Kinetics of the ionone synthesis on Brønsted acid solid catalysts*

Based on the previously discussed catalytic results and the reaction sequence depicted in Scheme 1, a heterogeneous kinetic model was postulated in order to interpret the catalytic results. Thus, seven catalytic runs were modeled with a total of ≈ 364 data points, comprising the experiments at 353 K varying the strength of the Brønsted acid sites (samples HPAS-59, TFAS and Amberlyst 35W) and the reaction temperature on HPAS-59. Our goal was to calculate the kinetic constants (k_i) for the reaction steps depicted in Scheme 1 and to analyze their dependence on the catalyst acid properties and reaction temperature.

The kinetic study was carried out using a Langmuir-Hinshelwood-Hougen- Watson (LHHW) heterogeneous model with the following assumptions:

- The only products of the pseudoionone (PS) conversion are α-, β- and γ-ionones.
- PS and ionones interact with a single Brønsted acid site (H^+) present on the surface of HPAS-59, TFAS and Amberlyst 35W.
- α-, β- and γ-ionones are obtained from the Int surface species in parallel reactions.
- The adsorption constants of α-, β- and γ-ionones are equivalent ($K_\alpha = K_\beta = K_\gamma = K$).
- γ-ionone isomerizes to α-ionone and/or β-ionone.
- The surface reaction steps are irreversible and rate-limiting.

Based on the assumptions given above, the following mechanism with nine reaction steps (steps *I* to *IX*) is postulated:

$$PS + * \leftrightarrow Int* \quad K_{Int} = \frac{C_{Int*}}{C_{PS}C_*} \tag{I}$$

$$Int* \rightarrow \alpha* \quad r_{II} = k'_{II}C_{Int*} \tag{II}$$

$$Int* \rightarrow \beta* \quad r_{III} = k'_{III}C_{Int*} \tag{III}$$

$$Int* \rightarrow \gamma* \quad r_{IV} = k'_{IV}C_{Int*} \tag{IV}$$

$$\gamma* \rightarrow \alpha* \quad r_V = k'_V C_{\gamma*} \tag{V}$$

$$\gamma* \rightarrow \beta* \quad r_{VI} = k'_{VI}C_{\gamma*} \tag{VI}$$

$$\alpha* \leftrightarrow \alpha + * \quad K'_\alpha = \frac{1}{K_\alpha} = \frac{C_\alpha C_*}{C_{\alpha*}} \tag{VII}$$

$$\beta* \leftrightarrow \beta + * \quad K'_\beta = \frac{1}{K_\beta} = \frac{C_\beta C_*}{C_{\beta*}} \tag{VIII}$$

$$\gamma* \leftrightarrow \gamma + * \quad K'_\gamma = \frac{1}{K_\gamma} = \frac{C_\gamma C_*}{C_{\gamma*}} \tag{IX}$$

where: PS is pseudoionone in the liquid phase; ∗ is a surface proton site (H^+); Int ∗ is the surface cyclic intermediate obtained by PS protonation; α ∗, β ∗ and γ ∗ are the three surface ionone species; α, β and γ are the ionone isomers in the liquid phase.

A simplified reaction network depicted in Scheme 2 was used in which the subscripts of the kinetic constants refer to the reaction step numbers of Scheme 1. Based on Scheme 2, the mass balances for the different components of the reaction mixture were written as shown in the differential Eqs. (5)–(8):

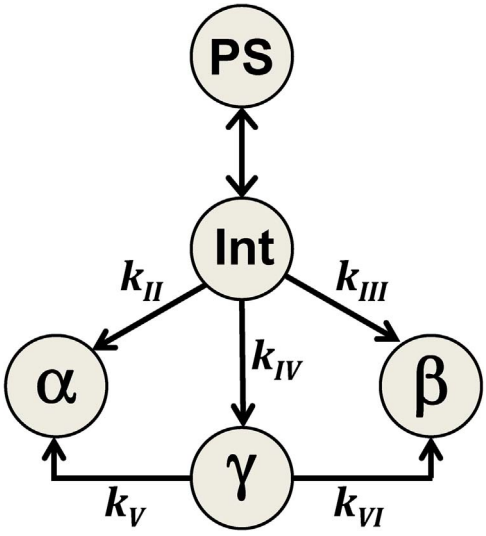

Scheme 2. Simplified reaction pathways for pseudoionone conversion used for kinetic modeling. Step numbers as in Scheme 1.

$$\frac{n^0_{PS}}{W}\frac{dC^*_{PS}}{dt} = -r_{II} - r_{III} - r_{IV} \tag{5}$$

$$\frac{n^0_{PS}}{W}\frac{dC^*_{\alpha}}{dt} = r_{II} + r_V \tag{6}$$

$$\frac{n^0_{PS}}{W}\frac{dC^*_{\beta}}{dt} = r_{III} + r_{VI} \tag{7}$$

$$\frac{n^0_{PS}}{W}\frac{dC^*_{\gamma}}{dt} = r_{IV} - r_V - r_{VI} \tag{8}$$

where r_{II}, r_{III}, r_{IV}, r_V and r_{VI} are the reaction rates of steps *II, III, IV, V* and *VI* respectively, expressed in mmol/h g; and C^*_j is the relative concentration of compound *j* (C_j/C^0_{PS}).

The mathematical expressions for the reaction rates of each step are:

$$r_{II} = \frac{k_{II}K_{Int}C_{PS}}{1 + K_{Int}C_{PS} + K(C_\alpha + C_\beta + C_\gamma)} \tag{9}$$

$$r_{III} = \frac{k_{III}K_{Int}C_{PS}}{1 + K_{Int}C_{PS} + K(C_\alpha + C_\beta + C_\gamma)} \tag{10}$$

$$r_{IV} = \frac{k_{IV}K_{Int}C_{PS}}{1 + K_{Int}C_{PS} + K(C_\alpha + C_\beta + C_\gamma)} \tag{11}$$

$$r_V = \frac{k_V C_\gamma K}{1 + K_{Int}C_{PS} + K(C_\alpha + C_\beta + C_\gamma)} \tag{12}$$

$$r_{VI} = \frac{k_{VI} C_\gamma K}{1 + K_{Int}C_{PS} + K(C_\alpha + C_\beta + C_\gamma)} \tag{13}$$

where k_{II}, k_{III}, k_{IV}, k_V and k_{VI} are kinetic parameters expressed in mmol/hg that involve the total active site concentration (C^T_*) on the catalyst surface:

$$C^T_* = C_* + C_{Int*} + C_{\alpha*} + C_{\beta*} + C_{\gamma*} \tag{14}$$

Initially, the modeling was performed for the experiments on HPAS-59 at different temperatures, Fig. 3. Thus, the kinetic constant dependence on the reaction temperature according to the Arrhenius law is given in Eqs. (15)–(19):

$$k_{II} = k_{IITr}\exp\left[\frac{-E_{II}}{R}\left(\frac{1}{T} - \frac{1}{T_r}\right)\right] \tag{15}$$

$$k_{III} = k_{IIITr}\exp\left[\frac{-E_{III}}{R}\left(\frac{1}{T} - \frac{1}{T_r}\right)\right] \tag{16}$$

$$k_{IV} = k_{IVTr}\exp\left[\frac{-E_{IV}}{R}\left(\frac{1}{T} - \frac{1}{T_r}\right)\right] \tag{17}$$

$$k_V = k_{VTr}\exp\left[\frac{-E_V}{R}\left(\frac{1}{T} - \frac{1}{T_r}\right)\right] \tag{18}$$

$$k_{VI} = k_{VITr}\exp\left[\frac{-E_{VI}}{R}\left(\frac{1}{T} - \frac{1}{T_r}\right)\right] \tag{19}$$

where $T_r = 353$ K is a reference temperature; E_i are the activation energies for each reaction step and k_{iTr} is given by:

$$k_{iTr} = A_i\exp\left[\frac{-E_i}{RT_r}\right] \tag{20}$$

where A_i is the frequency factor of the Arrhenius equation.

Eqs. (5)–(19) were solved numerically as described in Section 2.4 for the experiments of Fig. 3. The calculations were initially carried out for the whole set of reaction steps depicted in Scheme 2, i.e, considering that on the HPA-based catalyst γ-ionone could be isomerized to both α- and β-ionone. However, the best fit, i.e. the highest model selection criterion value (*MSC* ≈ 5.53, Eq. (3)), was obtained when γ- to β-

Table 3
Kinetic and statistical parameters obtained during PS cyclization on HPAS-59 at different reaction temperatures.

Reaction step	E_i (Kcal/mol)	A_i (mmol/hg)
II	18.2 ± 1.7	$2.0x10^{11}$ ± 10.1
III	16.6 ± 1.1	$1.1x10^{10}$ ± 4.9
IV	15.1 ± 1.0	$2.7x10^{9}$ ± 4.2
V	18.1 ± 2.4	$1.3x10^{11}$ ± 25.2
VI	–	–

MSC = 5.53, SSE = 0.0132, R^2 = 0.998.

ionone conversion was not included in the reaction network (k_{VI} = 0), in agreement with the conclusions of Section 3.2.3.

The primary kinetic parameters obtained from PS cyclization modeling on HPAS-59 at different reaction temperatures, i.e., the activation energy (E_i) and frequency factor (A_i) of each reaction step are given in Table 3. The E_i values are similar to the value reported by Kashid et al. [8] for the α- to β-ionone isomerization homogeneously promoted by sulfuric acid. Clearly, formation of the three ionone isomers proceeds with similar E_i values on the HPA-based catalyst. However, E_{II} (α-ionone formation) is slightly higher than those of the other isomers and similar to that of the γ- to α-ionone isomerization reaction (E_V). This indicates that an increase of the reaction temperature on HPAS-59 will increase the α-ionone selectivity due to the combined contribution of the primary and secondary reaction pathways (step *II* and step *V*, Scheme 1) that occur with comparable activation energies. In fact, this was found experimentally when ionone isomer distribution was compared at different temperatures and at $X_{PS} \approx 40\%$ [5], but the data at other conversion levels show similar trends.

Fig. 3 shows the good agreement between the experimental data obtained on HPAS-59 at 343, 353, 363, 373 and 383 K (symbols) and the kinetic model prediction (solid lines). In addition, Table 4 (entries 1–5), presents the corresponding kinetic constants for each reaction step calculated using the kinetic parameters shown in Table 3. Results show that the kinetic constants of the reaction steps leading to α- and γ-ionone (k_{II} and k_{IV}, respectively) duplicate the value of that of β-ionone formation (k_{III}), regardless of the reaction temperature. Thus, the modeling results indicate that on HPAS-59 the direct formations of α- and γ-ionone from PS are more favored than that of β-ionone, in agreement with the experimental results of Fig. 3.

The catalytic results obtained during ionone synthesis at 353 K on Brønsted solids with different proton site strength (HPAS-59, TFAS and Amberlyst 35W) were also modeled. Results are given as solid lines in Fig. 1 and in entries 2, 6 and 7 of Table 4. Again, the good agreement between experimental and model results confirms that the proposed LHHW heterogeneous model is suitable for interpreting the catalytic performance of different solid acids.

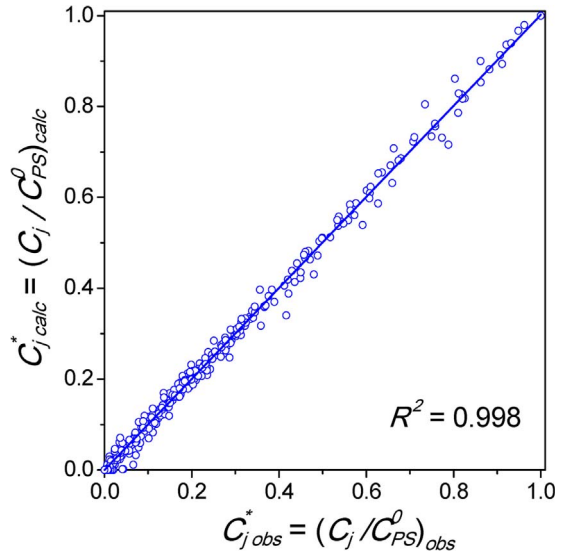

Fig. 4. Parity plot of the experimental ($C^*_{jobs} = (C_j/C^0_{PS})_{obs}$) and predicted ($C^*_{jcalc} = (C_j/C^0_{PS})_{calc}$) relative concentrations of PS and ionones.

The TFAS sample exhibits the highest values for the kinetic parameters (entry 6, Table 4) involved in the direct synthesis of α (k_{II}), β (k_{III}) and γ isomers (k_{IV}) from PS. In fact, the values of k_{II}, k_{III} and k_{IV} on TFAS are ≈ 4 times higher than on Amberlyst 35W (entry 7) and more than 15 times higher than the parameters calculated for HPAS-59 (entry 2). These results are in agreement with the initial activity (r^0_{IONONE}) order found for the three catalysts (Table 2). On the other hand, the results of Fig. 1 are congruent with the kinetic constant values calculated for the γ-ionone isomerization steps, showing that γ- to β-ionone conversion (k_{VI}) occurs at much higher rate on the catalyst having the strongest Brønsted acid sites (TFAS), while transformation of γ-ionone into the α isomer (k_V) is more favored on the Amberlyst resin.

A parity plot contrasting the 364 experimental ($C^*_{jobs} = (C_j/C^0_{PS})_{obs}$) and calculated ($C^*_{jcalc} = (C_j/C^0_{PS})_{calc}$) relative concentrations of the reaction mixture components is given in Fig. 4. The resulting linear correlation with a R^2 value of 0.998 indicates that the heterogeneous LHHW model well represents the reaction system and the experimental data obtained after testing three different catalysts at five different reaction conditions. Furthermore, Tables 3 and 4 show the values of the objective function (*SSE*) and the coefficient of determination (R^2) for each catalyst. The *SSE* was minimized in all cases at values ranging

Table 4
Kinetic constants and statistical parameters obtained during PS cyclization on HPAS-59, TFAS and Amberlyst 35W resin.

Entry	Catalyst	Reaction temperature (K)	Kinetic constants (mmol $h^{-1}g^{-1}$)				
			α	β	γ	γ → α	γ → β
			k_{II}	k_{III}	k_{IV}	k_V	k_{VI}
1	HPAS-59[a]	343	0.57	0.31	0.69	≈ 0.00	–
2		353	0.95	0.59	1.16	0.70	–
3		363	1.73	1.06	2.13	1.93	–
4		373	5.22	2.62	4.69	2.63	–
5		383	8.04	3.51	6.16	5.96	–
6	TFAS[b]	353	14.96 ± 6.28	9.74 ± 3.95	17.83 ± 7.72	0.88 ± 0.78	8.14 ± 1.31
7	Amberlyst 35W[c]	353	4.31 ± 0.90	2.53 ± 0.59	3.97 ± 0.41	4.49 ± 0.90	1.17 ± 0.88

[a] See statistical parameters of HPAS-59 kinetic modeling in Table 3.
[b] Statistical parameters of TFAS kinetic modeling: MSC = 5.24, SSE = 0.0096, R^2 = 0.996.
[c] Statistical parameters of Amberlyst kinetic modeling: MSC = 4.85, SSE = 0.0157, R^2 = 0.994.

from 9.60×10^{-3} and 1.57×10^{-2}, whereas R^2 takes satisfactory values close to unity.

4. Conclusions

The kinetics and mechanism of the ionone synthesis (α, β and γ isomers) from pseudoionone were studied on different Brønsted acid catalysts. Based on the catalytic results, a heterogeneous Langmuir-Hinshelwood-Hougen-Watson kinetic model was postulated to interpret the experimental data obtained on HPA/SiO_2, TFA/SiO_2 and resin Amberlyst 35W. The reaction mechanism starts by the adsorption of pseudoionone on Brønsted acid sites forming a cyclic cationic intermediate from which the three ionone isomers form in parallel pathways with similar activation energies. Then, the least stable γ-ionone isomer is converted to the other isomers, thereby improving the final selectivity to most valuable α- and β-ionones.

The LHHW modeling of the set of elementary steps involved in the proposed reaction mechanism predicts and explains, with physical meaning, the patterns of selectivity and activity experimentally determined on the catalysts for pseudoionone conversion. For example, the kinetic constants determined from the LHHW model predict that the direct formations of α- and γ-ionone from pseudoionone on HPA/SiO_2 are more favored than that of β-ionone, in agreement with the experimental data. Furthermore, the model successfully interprets the effect of both temperature and Brønsted acid strength on catalyst selectivity, i.e. on ionone isomer distribution.

Acknowledgements

Authors thank the Agencia Nacional de Promoción Científica y Tecnológica (ANPCyT), Argentina (Grant PICT 1888/10), CONICET, Argentina (grant PIP 11220090100203/10) and Universidad Nacional del Litoral, Santa Fe, Argentina (grant CAID PI 007-040/05) for financial support of this work.

References

[1] Ullmann's Encyclopedia of Industrial Chemistry, Sixth edition, (2002) (electronic).
[2] E. Brenna, C. Fuganti, S. Serra, P. Kraft, Eur. J. Org. Chem. (2002) 967.
[3] H. Hibbert, L.T. Cannon, J. Am Chem. Soc. 46 (1924) 119.
[4] V.K. Díez, C.R. Apesteguía, J.I. Di Cosimo, Catal. Lett. 123 (2008) 213.
[5] V.K. Díez, B.J. Marcos, C.R. Apesteguía, J.I. Di Cosimo, Appl. Catal. A: Gen. 358 (2009) 95–102.
[6] V.K. Díez, C.R. Apesteguía, J.I. Di Cosimo, Catal. Today 149 (2010) 267–274.
[7] E. Earl Royalds, Ind. Eng. Chem. 38 (5) (1946) 546–548.
[8] M.N. Kashid, I. Yuranov, P. Raspail, P. Prechtl, J. Membrez, A. Renken, L. Kiwi-Minsker, Ind. Eng. Chem. Res. 50 (2011) 7920–7926.
[9] H. Freund, M.L. Wright, R.K. Brookshier, Anal. Chem. 23 (5) (1951) 781.
[10] R.E. Walpole, R.H. Myers, S.L. Myers, K.E. Ye, Probability & Statistics for Engineers & Scientists, 8th Edition, (2007).
[11] S. Armenise, E. García-Bordeje, J.L. Valverde, E. Romeo, A. Monzón, Phys. Chem. Chem. Phys. 15 (2013) 12104–12117.
[12] A. de Angelis, C. Flego, P. Ingallina, L. Montanari, M.G. Clerici, C. Carati, C. Perego, Catal. Today 65 (2001) 363.
[13] C. Morterra, A. Chiorino, G. Ghiotti, E. Fisicaro, J. Chem. Soc. Faraday Trans. I 78 (1982) 2649.
[14] C.K. Jørgensen, Naturwissenschaften 67 (1980) 188.
[15] T. Okuhara, M. Misono, Encyclopedia of Organic Chemistry, in: R.B. King (Ed.), John Wiley and Sons, 1994.
[16] R. Bringué, M. Iborra, J. Tejero, J.F. Izquierdo, F. Cunill, C. Fité, V.J. Cruz, J. Catal. 244 (2006) 33.
[17] R. Rachwalik, P. Michorczyk, J. Ogonowski, Catal. Lett. 141 (2011) 1384–1390.